Ground-State Thermodynamic Quantities of Homogeneous Spin-1/2 Fermions from the BCS Region to the Unitarity Limit

Munekazu Horikoshi,[1,2] Masato Koashi,[1,2,3] Hiroyuki Tajima,[4] Yoji Ohashi,[4] and Makoto Kuwata-Gonokami[1,2,5]

[1]*Institute for Photon Science and Technology, Graduate School of Science, The University of Tokyo, 7-3-1 Hongo, Bunkyo-ku, Tokyo 113-8656, Japan*

[2]*Photon Science Center, Graduate School of Engineering, The University of Tokyo, 2-11-16 Yayoi, Bunkyo-ku, Tokyo 113-8656, Japan*

[3]*Department of Applied Physics, Graduate School of Engineering, The University of Tokyo, 7-3-1 Hongo, Bunkyo-ku, Tokyo 113-8656, Japan*

[4]*Department of Physics, Keio University, 3-14-1 Hiyoshi, Kohoku-ku, Yokohama 223-8522, Japan*

[5]*Department of Physics, Graduate School of Science, The University of Tokyo, 7-3-1 Hongo, Bunkyo-ku, Tokyo 113-0033, Japan*

(Received 14 December 2016; revised manuscript received 30 April 2017; published 11 October 2017)

The understanding of physical properties of fermions in the unitary regime, where the *s*-wave scattering length in the collisional channel of particles is longer than both the interparticle distance and the size of the interaction potential, is a crucial issue for electron systems of high-temperature superconductivity, dilute nucleons in nuclei, and neutron stars. We experimentally determine various thermodynamic quantities of interacting two-component fermions at the zero-temperature limit from the BCS region to the unitarity limit. The obtained results are very accurate in the sense that the systematic error is within 4% in the unitary regime. Using this advantage, we can compare our data with various many-body theories. We find that an extended T-matrix approximation, which is a strong-coupling theory involving fluctuations in the Cooper channel, well reproduces our experimental results. We also find that the superfluid order parameter Δ calculated by solving the ordinary BCS gap equation with the chemical potential of interacting fermions is close to the binding energy of the paired fermions directly observed in a spectroscopic experiment and that obtained using a quantum Monte Carlo method.

DOI: 10.1103/PhysRevX.7.041004

Subject Areas: Atomic and Molecular Physics, Condensed Matter Physics, Nuclear Physics

I. INTRODUCTION

A many-body system of fermions interacting with *s*-wave scattering length a is a fundamental model that extends the ideal Fermi gas model for various interacting Fermi systems. Understanding the ground-state properties of fermions in the unitary regime, where the absolute value of the scattering length is larger than the interparticle distance, is crucial in condensed-matter physics and nuclear physics, beyond the framework of atomic, molecular, and optical physics.

Ultracold atomic gases provide an ideal research environment in which we can investigate such many-body Fermi systems universally and systematically [1–3]. Many-body systems composed of ultracold atoms have an ideal hierarchy of length and energy, where the interparticle distance and the wavelength of matter are sufficiently long compared to the size of the short-range interaction potential. Furthermore, it is possible to tune the scattering length between two fermions using Feshbach resonances [4]. These features realize universal many-body systems, where various physical phenomena are independent of the details of particles [5].

The ground state of many-body fermions interacting with an *s*-wave scattering length is an *s*-wave superfluid state, which has a nonzero superfluid order parameter Δ of the paired fermions and fluctuations of the order parameter. The origin of such superfluid fluctuations is the repetition of pair formations and their dissociations as well as noncondensed pairs that are kicked out from the condensate. Far below the superfluid phase transition temperature T_c, where thermal excitations are almost absent, many-body corrections to physical quantities are dominated by quantum fluctuations associated with superfluid fluctuations.

At the BCS limit, the BCS mean-field (MF) wave function has been considered to be an adequate approximation to describe the ground-state properties because the influence of quantum fluctuations appears to be small due to weak interaction between fermions. In this BCS-MF approximation, the magnitude of the order parameter Δ is

equivalent to the binding energy of a paired fermion and to the energy gap in single-particle excitations [6]. The relation between the thermodynamic quantities and Δ is given by the gap equation and the number equation. The influence of quantum fluctuations on the ground-state energy has also been theoretically analyzed at the BCS limit. The thermodynamic quantities of such fermions have been expressed analytically up to the order of $(k_F a)^2$ beyond the MF approximation [7].

In the unitary regime, on the other hand, it is not obvious whether the BCS-MF wave function is an adequate approximation for describing the ground-state properties because considerable quantum fluctuations are induced by strong interaction between fermions. While there are several exact universal relations among the thermodynamic quantities [8–13], they cannot link thermodynamic quantities to the order parameter, the binding energy of a paired fermion, and the superfluid fluctuations. Thus far, the binding energy of a paired fermion [14], a single-particle excitation spectrum [15–17], and internal energy density $\mathcal{E}$ [18], which is the ground-state energy per unit volume, have been experimentally determined in the unitary regime. Other thermodynamic quantities, such as pressure [18,19], isothermal compressibility [19,20], speed of sound [21], and contact density [17], were also measured. However, the magnitude of the order parameter and chemical potential μ have not yet been determined experimentally in the unitary regime. While several theories have demonstrated qualitative agreement with these experimental results, quantitative evaluation of these theories has not been achieved because of experimental accuracies, lack of data points, and inhomogeneity effects.

In the present study, we determine the relations among thermodynamic quantities, such as pressure P, number density n, internal energy density $\mathcal{E}$, chemical potential μ, isothermal compressibility κ, and contact density $\mathcal{C}$, for homogeneous spin-1/2 superfluid fermions at the zero-temperature limit from the BCS region to the unitarity limit. All of these quantities are determined within 4% systematic error around the unitarity limit without using any model functions. We provide their thermodynamic functions in universal form as a function of an interaction parameter. Therefore, these functions are applicable to other similar many-body Fermi systems, such as dilute neutron matter. We compare our experimental data with various many-body theories and find that one theoretical model can reproduce our data. We also calculate the superfluid order parameter by solving the ordinary BCS gap equation with the determined chemical potential. We compare the obtained results with the binding energies of paired fermions, which were determined in previous studies through a spectroscopic experiment and quantum Monte Carlo (QMC) calculation.

The remainder of the present paper is organized as follows. In Sec. II, we introduce the theoretical framework used in our data analysis. In Sec. III, we explain our experimental procedure, data analysis, and experimental results. In Sec. IV, we compare our experimental results with the results of various previous experimental and theoretical studies and discuss calculation of the superfluid order parameter. Finally, in Sec. V, we conclude this study.

II. THEORETICAL FRAMEWORK

A. Thermodynamics of homogeneous fermions from the BCS limit to the unitarity limit at zero temperature

We consider homogeneous spin-1/2 fermions at $T = 0$, which have a number density of $n_\uparrow = n_\downarrow = n/2$ and a chemical potential of $\mu_\uparrow = \mu_\downarrow = \mu$ for each spin state. We assume that the interaction between fermions in different spin states is modeled by the s-wave scattering length a. In the following, for convenience, we use a^{-1} instead of a. We consider the parameter region $a^{-1} \leq 0$, where the Fermi system ranges from the BCS limit ($a^{-1} = -\infty$) to the unitarity limit ($a^{-1} = 0$). Let m be the mass of the fermions and let $\hbar$ be the reduced Plank constant.

The internal energy density $\mathcal{E}(n, a^{-1})$ is a function of n and a^{-1}. Let us write its differential form as

$$d\mathcal{E} = \mu dn - \left(\frac{\hbar^2}{4\pi m}\mathcal{C}\right) da^{-1}. \tag{1}$$

The thermodynamic quantity $\mathcal{C}$ defined in the above relation is called the contact density [8–13]. The pressure P is derived from $\mathcal{E}(n, a^{-1})$ as

$$P = \mu n - \mathcal{E}. \tag{2}$$

The functional dependence $P(\mu, a^{-1})$ has a simple differential form:

$$dP = n d\mu + \left(\frac{\hbar^2}{4\pi m}\mathcal{C}\right) da^{-1}. \tag{3}$$

Isothermal compressibility κ and speed of sound v have the same thermodynamic relations as an ideal Fermi gas under a fixed scattering length:

$$\kappa = \frac{1}{n}\left(\frac{\partial n}{\partial P}\right)_{a^{-1}} = \frac{1}{n^2}\left(\frac{dn}{d\mu}\right)_{a^{-1}} \tag{4}$$

$$v = \sqrt{\frac{1}{mn\kappa}}. \tag{5}$$

B. Dimensionless thermodynamic functions

Here, we use the fact that the theory involves only two constants, m and $\hbar$. If we change the unit of length by a factor of λ and that of time by λ^2, the values of the two constants remain unchanged. Hence, the functional dependence of any dimensionless qualities A on n and

a^{-1} should satisfy $A(n,a^{-1}) = A(\lambda^3 n, \lambda a^{-1})$. This implies that A can be written as a function $A(x)$ of a parameter x proportional to $a^{-1}n^{-1/3}$ [5]. Similarly, when a dimensionless quantity B is a function of μ and a^{-1}, it should be written as a function $B(X)$ of a parameter X proportional to $a^{-1}\mu^{-1/2}$.

In the present paper, we choose the two parameters to be the grand-canonical interaction parameter,

$$X(\mu, a^{-1}) = \frac{1}{k_\mu(\mu)a}, \tag{6}$$

and the canonical interaction parameter,

$$x(n, a^{-1}) = \frac{1}{k_F(n)a}. \tag{7}$$

Here, we define two wave numbers as $k_\mu(\mu) = \sqrt{2m\mu}/\hbar$ and $k_F(n) = \sqrt{2m\varepsilon_F(n)}/\hbar$, where $\varepsilon_F(n) = (\hbar^2/2m)(3\pi^2 n)^{2/3}$ is the Fermi energy for ideal fermions. For each thermodynamic quantity, we define an associated dimensionless thermodynamic function by normalizing it with the value for an ideal Fermi gas as follows:

$$\text{pressure: } f_P(X) = \frac{P}{P_0(\mu)}, \tag{8}$$

$$\text{number density: } f_n(X) = \frac{n}{n_0(\mu)}, \tag{9}$$

$$\text{internal energy density: } f_\mathcal{E}(x) = \frac{\mathcal{E}}{\mathcal{E}_0(n)}, \tag{10}$$

$$\text{chemical potential: } f_\mu(x) = \frac{\mu}{\varepsilon_F(n)}, \tag{11}$$

$$\text{isothermal compressibility: } f_\kappa(x) = \frac{\kappa}{\kappa_0(n)}, \tag{12}$$

$$\text{speed of sound: } f_v(x) = \frac{v}{v_0(n)}, \tag{13}$$

where $P_0(\mu) = (2/15\pi^2)(2m/\hbar^2)^{3/2}\mu^{5/2}$, $n_0(\mu) = \frac{5}{2}[P_0(\mu)/\mu]$, $\mathcal{E}_0(n) = \frac{3}{5}n\varepsilon_F(n)$, $\kappa_0(n) = \frac{3}{2}(1/n\varepsilon_F(n))$, and $v_0(n) = [(mn\kappa_0(n)]^{-1/2}$. An exception is the contact density $\mathcal{C}$, which vanishes for the ideal gas. Here, we choose its dimensionless thermodynamic function as

$$\text{contact density: } f_\mathcal{C}(x) = \frac{\mathcal{C}}{k_F(n)^4}. \tag{14}$$

In an experiment with interacting Fermi gas in a trap potential in Sec. III, we obtain data including various combinations of (μ, P) with a fixed value of the scattering length a. It is convenient for data analysis to introduce dimensionless versions of μ and P by using normalizing factors solely determined from a as

$$\mathcal{G} = \frac{\mu}{\varepsilon_a}, \qquad \chi = P\frac{a^3}{\varepsilon_a}, \tag{15}$$

where we define energy as $\varepsilon_a = (\hbar^2/2ma^2)$. According to the dimensionless analysis discussed above, we can see that $\mathcal{G}$ is given as a function of χ, i.e., $\mathcal{G}(\chi)$. Since X and f_P are simply related to $\mathcal{G}(\chi)$ as

$$X = -\mathcal{G}(\chi)^{-1/2}, \qquad f_P = -\frac{15\pi^2}{2}\chi\mathcal{G}(\chi)^{-5/2}, \tag{16}$$

$\mathcal{G}(\chi)$ can be directly converted to $f_P(X)$.

The function $f_n(X)$ is derived from $f_P(X)$ as

$$f_n(X) = f_P(X) - \frac{X}{5}\frac{df_P(X)}{dX}. \tag{17}$$

The function $f_\mathcal{E}(x)$ is constructed by

$$f_\mathcal{E} = \frac{5f_n(X) - 2f_P(X)}{3f_n^{5/3}(X)}, \qquad x = Xf_n(X)^{-1/3}. \tag{18}$$

The function $f_\mu(x)$ is derived from $f_\mathcal{E}(x)$ as

$$f_\mu(x) = f_\mathcal{E}(x) - \frac{x}{5}\frac{df_\mathcal{E}(x)}{dx}. \tag{19}$$

When $f_\mu(x)$ is given, $f_\kappa(x)$ can be determined by

$$f_\kappa(x) = \left\{f_\mu(x) - \frac{x}{2}\frac{df_\mu(x)}{dx}\right\}^{-1}. \tag{20}$$

The function $f_v(x)$ has a simple relation to $f_\kappa(x)$:

$$f_v(x) = f_\kappa(x)^{-1/2}. \tag{21}$$

The function $f_\mathcal{C}(x)$ is obtained from the derivative of $f_\mathcal{E}(x)$ as

$$f_\mathcal{C}(x) = -\frac{2}{5\pi}\frac{df_\mathcal{E}(x)}{dx}. \tag{22}$$

Equations (17)–(20) indicate that there is a universal value ξ at the unitarity limit ($X = x = 0$), which is $\xi = f_P(0)^{-2/3} = f_n(0)^{-2/3} = f_\mathcal{E}(0) = f_\mu(0) = f_\kappa(0)^{-1}$. Note that ξ is sometimes called the Bertsch parameter [1].

C. Behavior of the dimensionless functions at the BCS limit

The asymptotic behavior of $f_\mathcal{E}(x)$ at the BCS limit is known up to the second order of $1/x$ [7,22] as

$$f_{\mathcal{E}}^{\mathrm{asym}}(x\to-\infty)=1+\frac{10}{9\pi}x^{-1}+\frac{4(11-2\log 2)}{21\pi^2}x^{-2}. \quad (23)$$

Here, we omit the condensation energy term [7]. Moreover, $f_{\mu}^{\mathrm{asym}}(x)$ is given by Eq. (19) with $f_{\mathcal{E}}^{\mathrm{asym}}(x)$, and $f_{P}^{\mathrm{asym}}(X)$ is obtained using the following relations:

$$f_P=\frac{5f_\mu(x)-3f_{\mathcal{E}}(x)}{2f_\mu^{5/2}(x)}, \qquad X=xf_\mu(x)^{-1/2}. \quad (24)$$

The asymptotic behavior of the other thermodynamic quantities at the BCS limit can be obtained from $f_{P}^{\mathrm{asym}}(X)$ using Eqs. (17)–(22).

III. EXPERIMENT

A. Data acquisition

We have an experimental apparatus that can produce dual Bose-Einstein condensates (BECs) of paired ^{6}Li (fermion) and one spin state of ^{7}Li (boson) in the hybrid trap of an optical dipole trap (ODT) and a magnetic trap (MT) [23]. A schematic drawing of the experimental apparatus is shown in Fig. 1. Detailed information about our experimental apparatus and experimental procedure is provided in a previous study [23]. In this experiment, only ^{6}Li atoms are used. The shape of the trapping potential U_{trap} is analytically given without using a harmonic approximation in terms of the parameters of the laser power, the wavelength, the beam waists of the ODT, and the magnetic curvature of the MT. The trap has an elliptic symmetry and can be written as $U_{\mathrm{trap}}(\hat{x},\hat{y},\hat{z})=U_{\mathrm{trap}}(\hat{\rho},\hat{z})$, with $\hat{\rho}=\sqrt{\hat{x}^2+\eta^2(\hat{z})\hat{y}^2}$, where $\eta(\hat{z})$ is the ellipticity, where the variables with hats mean the spatial coordinates.

The ODT is produced by a focused 1070-nm laser beam. The $1/e^2$ beam radii are $(w_{0\hat{x}},w_{0\hat{y}})=(43.5,46.9)$ μm, and the final laser power after evaporative cooling is $P_{\mathrm{ODT}}=45$ mW. The depth of the ODT is 38 μK, and the trapping frequency realized by the ODT is $(\omega_{\hat{x}},\omega_{\hat{y}},\omega_{\hat{z}})=2\pi\times(250,230,1.3)$ Hz. The MT is produced by the magnetic curvature of a bias magnetic field for the Feshbach resonance and produces magnetic curvature $\omega_{\mathrm{mag}}=2\pi\times0.24\sqrt{B}$ Hz in the $\hat{z}$ direction, where B is the produced bias magnetic field in gauss. The effective trapping frequency along the $\hat{z}$ direction is given by $\omega_{\hat{z},\mathrm{eff}}=\sqrt{\omega_{\hat{z}}^2+\omega_{\mathrm{mag}}^2}$. Typically, 2×10^5 degenerate fermions are prepared in this experiment.

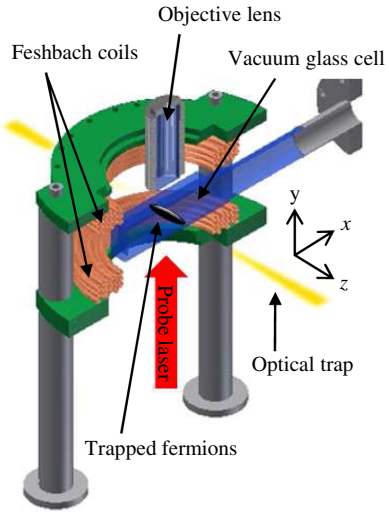

FIG. 1. Schematic diagram of the experimental apparatus. The $\hat{z}$ axis is defined as the axial direction of the optical trap.

^{6}Li atoms have a broad s-wave Feshbach resonance for collisions between the two lowest spin states: $|1\rangle\equiv|m_L=0,m_S=-1/2,m_I=+1\rangle$ and $|2\rangle\equiv|m_L=0,m_S=-1/2,m_I=0\rangle$, where m_L, m_S, and m_I are, respectively, the electronic orbital angular momentum projection, the electronic spin projection, and the nuclear spin projection. The scattering length is given by $a(B)=a_{\mathrm{bg}}[1+(W_{\mathrm{res}}/B-B_{\mathrm{res}})]$ with parameters of $a_{\mathrm{bg}}=-1582a_0$, $B_{\mathrm{res}}=832.18$ G, and $W_{\mathrm{res}}=262.3$ G, where a_0 is the Bohr radius [24,25]. Then, the Fermi system is in the BEC region ($a>0$) at $B<B_{\mathrm{res}}$. On the other hand, the Fermi system is in the BCS region ($a<0$) at $B>B_{\mathrm{res}}$. At $a(B=B_{\mathrm{res}})=\pm\infty$, the Fermi system reaches the unitarity limit.

In the present study, we are interested in the ground-state properties of the interacting fermions from the BCS limit to the unitarity limit. In order to prepare highly degenerate Fermi gas [$t=k_BT/\epsilon_F(n)\ll1$] in the interaction region, we produce an almost pure molecular BEC consisting of two fermions in the state of $|1\rangle$ and $|2\rangle$ at 777 G in the BEC regime. We then change the scattering length adiabatically by sweeping the magnetic field to 832.18–1050 G in 1.5 s.

We can accurately obtain their density distribution *in situ* using the imaging techniques developed in a previous study [26]. We measure the optical depth (OD) of the trapped fermions at each magnetic field, as shown in Fig. 2(a). From the OD and the absorption cross section σ_{abs}, we evaluate the column density $\bar{n}(\hat{x},\hat{z})=\int_{-\infty}^{+\infty}n(\hat{x},\hat{y},\hat{z})d\hat{y}$ by $\bar{n}(\hat{x},\hat{z})=\mathrm{OD}(\hat{x},\hat{z})/\sigma_{\mathrm{abs}}$. We determine the effective value of σ_{abs} within 4% uncertainty [26]. Note that this uncertainty results in one of the systematic errors in our final results.

The local pressure of the trapped fermions can be calculated from the column density $\bar{n}(\hat{x},\hat{z})$ and the trapping potential $U_{\mathrm{trap}}(\hat{\rho},\hat{z})$ using the following formula [26–28]:

$$P(\hat{\rho},\hat{z})=\frac{\eta(\hat{z})}{\pi}\int_{\hat{\rho}}^{\infty}d\hat{x}\,\bar{n}(\hat{x},\hat{z})\left[\frac{\frac{\partial U_{\mathrm{trap}}}{\partial\hat{\rho}}(\hat{x},\hat{z})}{(\hat{x}^2-\hat{\rho}^2)^{1/2}}+\int_{\hat{\rho}}^{\hat{x}}d\hat{\rho}'\frac{\hat{\rho}'\frac{\partial U_{\mathrm{trap}}}{\partial\hat{\rho}}(\hat{x},\hat{z})-\hat{x}\frac{\partial U_{\mathrm{trap}}}{\partial\hat{\rho}}(\hat{\rho}',\hat{z})}{(\hat{x}^2-\hat{\rho}'^2)^{3/2}}\right], \quad (25)$$

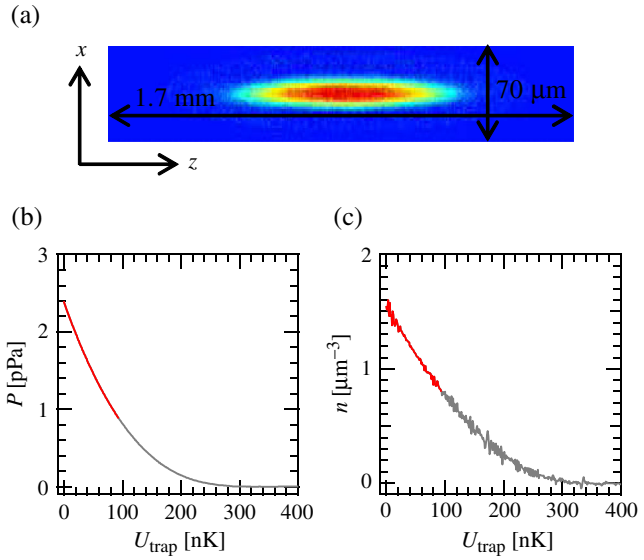

FIG. 2. Typical experimental data at 882.86 G. (a) Absorption image. (b) Local pressure $P(U_{\mathrm{trap}})$. (c) Local number density $n(U_{\mathrm{trap}})$. The red curves in (b) and (c) show the data region used in the analysis, where the number density is larger than half of the peak density.

which is derived from the Gibbs-Duhem equation [Eq. (3)], the local density approximation (LDA), i.e., $\mu = \mu_0 - U_{\mathrm{trap}}$, and the inverse Abel transformation of the column density, i.e., $n(\hat{\rho},\hat{z}) = -[\eta(\hat{z})/\pi]\int_{\hat{\rho}}^{\infty}(1/\sqrt{\hat{x}^2-\hat{\rho}^2})[\partial\bar{n}(\hat{x},\hat{z})/\partial\hat{x}]d\hat{x}$. This calculation can be carried out without the knowledge of the global chemical potential μ_0 of the trapped system. Finally, we can obtain pressure P as a function of the trapping potential U_{trap} by relating $P(\hat{\rho},\hat{z})$ and $U_{\mathrm{trap}}(\hat{\rho},\hat{z})$ at each position.

Figure 2(b) shows a typical example of $P(U_{\mathrm{trap}})$ at 882.86 G. The data are averaged at 241 potential heights in the region of $U_{\mathrm{trap}}/k_B \in [0, 600\ \mathrm{nK}]$ with an interval of $\Delta U_{\mathrm{trap}}/k_B = 2.5$ nK. We also evaluate the local number density from the local pressure $P(U_{\mathrm{trap}})$ according to $n(U_{\mathrm{trap}}) = -[dP(U_{\mathrm{trap}})/dU_{\mathrm{trap}}]$ under the LDA, as shown in Fig. 2(c).

We extract $P(U_{\mathrm{trap}})$ and $n(U_{\mathrm{trap}})$ in the highly degenerate region, where the number density is larger than half of the peak density for the following data analysis, because $t = k_B T/\varepsilon_F(n) \propto n^{-2/3}$. The red curves plotted in Figs. 2(b) and 2(c) show the regions. We acquire data sets of $\{P(U_{\mathrm{trap}}), n(U_{\mathrm{trap}}), a(B)^{-1}\}$ at 44 magnetic fields of from 832.54 to 1050 G for the BCS region and of 832.18 G for the unitarity limit. The 44 magnetic fields are chosen in order that the canonical interaction parameter $x[n(U_{\mathrm{trap}}), a(B)^{-1}]$ obtained at B overlaps one another. In this experiment, we repeat data acquisition 8 times at each magnetic field to decrease statistical errors.

We hereinafter express physical quantities at B by adding the superscript B, for example, P^B, n^B, and U^B_{trap}.

B. Evaluation of $f_\kappa(x)$

The dimensionless isothermal compressibility $f_\kappa(x)$ can be constructed model independently from data sets of $\{P^B(U^B_{\mathrm{trap}}), n^B(U^B_{\mathrm{trap}})\}$. We calculate $f^B_\kappa(U^B_{\mathrm{trap}})$ and $x^B(U^B_{\mathrm{trap}}, B)$ from these sets using the thermodynamic relation of Eq. (5) and the definitions of $x(n, a^{-1})$ and $\kappa_0(n)$. We collect $f^B_\kappa(x^B)$ from the BCS region to the unitarity limit and average the values at the given x, as shown by the red circles in Fig. 3. The error bars indicate the systematic errors in f_κ and x caused by the uncertainty of the absorption cross section σ_{abs}. From the error propagation rule, these errors are $(\delta f_\kappa/f_\kappa) = \frac{2}{3}(\delta\sigma_{\mathrm{abs}}/\sigma_{\mathrm{abs}}) = 2.7\%$ and $(\sigma x/x) = \frac{1}{3}(\delta\sigma_{\mathrm{abs}}/\sigma_{\mathrm{abs}}) = 1.3\%$. The statistical errors are within the error bars.

At the unitarity limit, our data indicate that $f_\kappa(0) = 2.66(7)$, which corresponds to the universal value of $\xi = 0.375(10)$. This value is very consistent with the accurate experimental value of 0.376(4) determined by measuring thermodynamics for homogeneous unitary Fermi gases [19]. In the BCS region, our data approach the theoretical asymptotic behavior of $f_\kappa(x)$.

Experimentally, it is impossible to prepare fermions at zero temperature, even if we start from a molecular BEC. Therefore, experimental temperature T_{expt} always has a nonzero value, i.e., $t_{\mathrm{expt}} > 0$. Since the superfluid critical temperature t_c decreases monotonically to zero from the unitarity limit to the BCS limit as a function of the interaction parameter x, it is inevitable that $t_c(x)$ intersects t_{expt} somewhere between the two interaction limits. Here, we define the transition point as $t_{\mathrm{expt}} = t_c(x^*)$.

Based on another experiment, as we describe in Appendix A, the transition point is determined to be

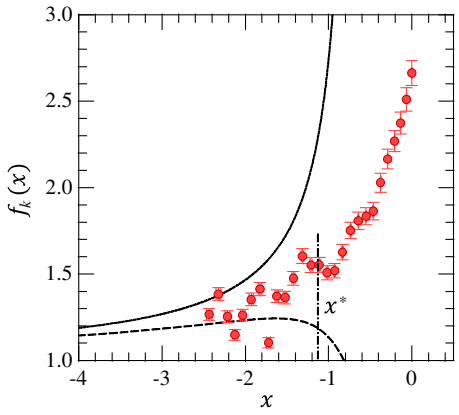

FIG. 3. Experimental data of isothermal compressibility from the BCS region to the unitarity limit. The red circles are experimental data. The dotted curve and the dashed curve show their asymptotic behavior at the BCS limit up to the first and second order of $1/x$, respectively. The vertical dash-dotted line indicates interaction parameter x^*, where superfluid transition occurs. The fermions are in the superfluid state in the region of $x > x^*$.

$x^* = -1.14$, and the temperature parameter of the fermions is estimated to be $0.06 \lesssim t_{\mathrm{expt}} \lesssim 0.1$ for our experimental condition. We indicate the superfluid transition point x^* with a vertical dash-dotted line in Fig. 3. In the region of $x > x^*$, the fermions are in the superfluid state. A cusp in $f_\kappa(x)$ appears around the transition point, as shown in Fig. 3, which is similar to that observed in a previous study [19].

C. Construction of $\mathcal{G}(\chi)$

In order to determine the other thermodynamic quantities, it is necessary to determine the chemical potential μ or contact density $\mathcal{C}$ along with P and n. In this experiment, we apply an almost homogeneous magnetic field to the gas, which implies that the Fermi gas has a homogeneous scattering length. In this case, it is impossible to determine $\mathcal{C}$ from the gradient of P relative to a^{-1} under the same μ for each data.

The local chemical potential μ^B is given by $\mu^B = \mu_0^B - U_{\mathrm{trap}}^B$ under the LDA, where μ_0^B is the global chemical potential at magnetic field B. If we have experimental data corresponding to the fermions in the ground state at the BCS limit, we can determine μ_0^B in such a way that $f_P(X)$ matches the asymptotic theory at the BCS limit. In this case, μ_0^B toward the unitarity limit can be determined by iterative fitting from the BCS limit with the same principle as demonstrated in a previous study [29]. However, as shown in Fig. 3, it is difficult to judge whether our data reach the BCS limit, and the data contain some finite-temperature effects at $x < x^*$ because the fermions are in the normal state there. Consequently, this method cannot be used to determine μ^B for our data.

Although the value of μ_0^B for each value of B is unknown, we can still determine the relative difference among the various values of B using the general properties of dimensionless parameters described in Sec. II B. Equation (15) and the LDA suggest that all of the experimental data acquired at various magnetic fields for the Feshbach resonance B should be related through a common function $\mathcal{G}(\chi)$ as

$$\mathcal{G}(\chi(U_{\mathrm{trap}}^B, B), B) = \frac{\mu_0^B - U_{\mathrm{trap}}^B}{\varepsilon_{a(B)}}, \tag{26}$$

where $\chi(U_{\mathrm{trap}}^B, B) = P^B(U_{\mathrm{trap}}^B)[a(B)^3/\varepsilon_{a(B)}]$. We plot $(\chi, \mathcal{G})$ with different choices of μ_0^B for all data in Fig. 4. In the case of $\mu_0^B = 0$ for all B, the plots do not overlap each other as the curves (i). However, we can overlap the plots model independently by simply adjusting each value of μ_0^B from the BCS limit ($B = 1050$ G) to the unitarity limit, as in the curves (ii). This leaves only a single ambiguous parameter, namely, the arbitrary choice of $\mu_0^{B=1050\ \mathrm{G}}$. As a result, the experimentally constructed value $\mathcal{G}(\chi)$ deviates from the true value $\mathcal{G}_{\mathrm{true}}(\chi)$ by a constant offset as $\mathcal{G}(\chi) = \mathcal{G}_{\mathrm{true}}(\chi) + \Delta\mathcal{G}$, where $\Delta\mathcal{G}$ is independent of χ.

We can derive a lower and an upper bound on the offset value in the following way. The contact density should be positive in the BCS-BEC crossover ($\mathcal{C} > 0$), and $\mathcal{C}$ is related to $f_P(X)$ by $(\mathcal{C}/k_\mu^4) = (4/15\pi)f_P'(X)$, which can be derived from Eq. (3). Then, $f_P(X)$ must have positive gradient $f_P'(X) > 0$ at an arbitrary interaction parameter X. This restriction gives the lower bound on $\mathcal{G}(\chi)$ through Eq. (16) as

$$\mathcal{G}(\chi) > \frac{5}{2}\chi\mathcal{G}'(\chi). \tag{27}$$

The border of this condition is plotted by the dash-dotted red curve in Fig. 4(a). This condition should be satisfied for the entire experimental curve $\mathcal{G}(\chi)$. The condition is most restrictive at $\chi_{\max} = -1.0 \times 10^{-4}$, which is the maximum value achieved in this experiment. Thus, the lower bound is given by $\mathcal{G}(\chi_{\max}) > 0.13$, which gives a lower bound on the experimental range of X from Eq. (16) as $X_{\min} > -2.77$.

In addition, the experimental data for f_P must satisfy the condition of $f_P > f_P(X_{\min})$ from the requirement of $f_P'(X) > 0$. This condition gives an upper bound on $\mathcal{G}(\chi)$ as

$$\mathcal{G}(\chi) < \left(-\frac{15\pi^2}{2f_P(X_{\min})}\chi\right)^{2/5} \tag{28}$$

for $\chi < \chi_{\max}$. In order to use the above inequality, we still need a lower bound on $f_P(X_{\min})$. Here, we invoke the theoretical asymptotic behavior to derive a bound that is better than the obvious bound of $f_P(X_{\min}) > 1$. We confirm that calculations of $f_P^{\mathrm{asym}}(X)$ up to the first and second orders of x^{-1} in Eq. (23) give almost the same values at $X = -5$, which is $f_P(X = -5) = 1.1$. By assuming that this value is reliable, we have the bound $f_P(X_{\min}) > 1.1$, because $X_{\min} > -5$. Using this bound, the condition of Eq. (28) is represented by the dashed red curve in Fig. 4(a). We confirm that the entire experimental curve $\mathcal{G}(\chi)$ lies below the red curve if and only if $\mathcal{G}(\chi_{\max}) < 0.14$.

Having established that $0.13 < \mathcal{G}(\chi_{\max}) < 0.14$, we choose the offset such that $\mathcal{G}(\chi_{\max}) = 0.135$, which is shown as curve (iii) in Fig. 4(a). This leads to a systematic error of $|\Delta\mathcal{G}| < 0.05$. Note that this constant uncertainty in the offset value becomes negligible toward the unitarity limit, because the value of $\mathcal{G}(\chi)$ around the unitarity limit is approximately 4 orders of magnitude larger than that around the BCS limit, as shown in Fig. 4. In terms of parameter X, the relative systematic error $|\Delta\mathcal{G}|/\mathcal{G}(\chi)$ is bounded by $0.05|X|^2$ because $\mathcal{G}(\chi) = |X|^{-2}$ from Eq. (16).

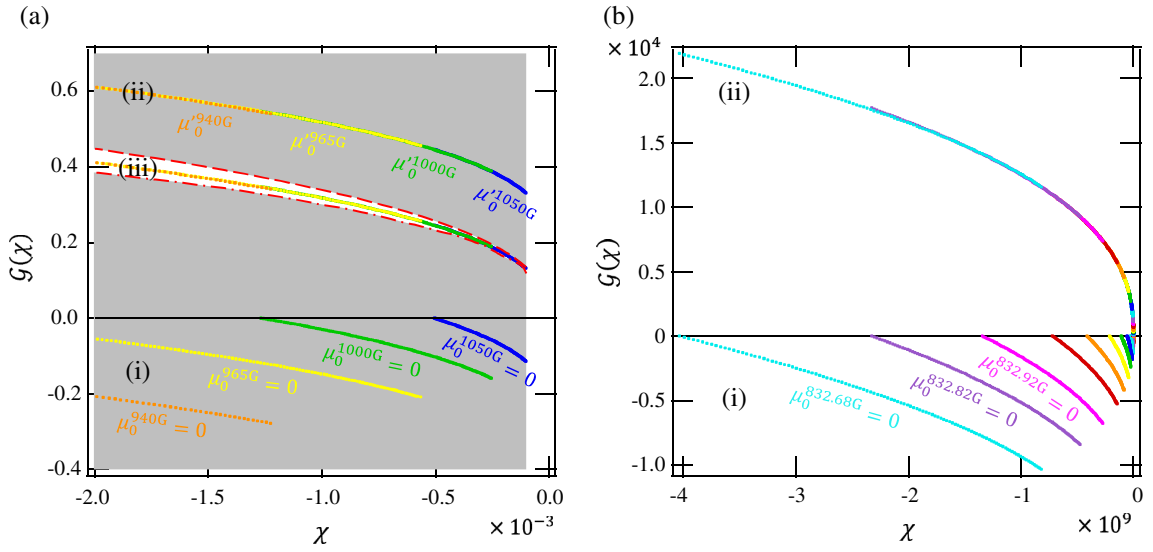

FIG. 4. Construction of dimensionless function $\mathcal{G}(\chi)$. The different colors indicate the contributions of data taken at each magnetic field for the Feshbach resonance. (a) Around the BCS limit. The dash-dotted red curve and the dashed red curve indicate the lower and upper limits of $\mathcal{G}(\chi)$. The gray areas correspond to the forbidden area for $\mathcal{G}(\chi)$. (i) Unconnected data with $\mu_0^B = 0$ for all data. (ii) Connected data located in the forbidden area. (iii) Connected data for which the offset value is tuned appropriately. (b) Around the unitarity limit. (i) Unconnected data with $\mu_0^B = 0$ for all data. (ii) Connected data for which the offset value is tuned appropriately.

D. Determination of $f_P(X)$, $f_n(X)$, $f_\mathcal{E}(x)$, $f_\mu(x)$, and $f_\mathcal{C}(x)$

We convert $\mathcal{G}(\chi)$ to $f_P(X)$ according to Eq. (16) and derive the other dimensionless functions from $f_P(X)$ using the thermodynamic relations of Eqs. (17)–(20). Figure 5 shows the results. The red regions indicate systematic errors caused by uncertainty $\Delta\mathcal{G}$ for determining the offset value of $\mathcal{G}(\chi)$, which depend on X. The blue regions indicate systematic errors caused by uncertainty of the absorption cross section $\sigma_{\rm abs}$, which do not depend on X. In the interaction region of $X > -0.18$ or $x > -0.12$, the former errors become 1 order smaller than the latter. Therefore, all of the thermodynamic quantities are determined by the uncertainty of $\sigma_{\rm abs}$ as $(\delta f_P/f_P) = (\delta f_n/f_n) = (\delta\sigma_{\rm abs}/\sigma_{\rm abs}) = 4\%$ and $(\delta f_\mathcal{E}/f_\mathcal{E}) = (\delta f_\mu/f_\mu) = \frac{2}{3}(\delta\sigma_{\rm abs}/\sigma_{\rm abs}) = 3\%$ around the unitarity limit.

We find that the superfluid transition point corresponds to $X^* = -1.33$ at $x^* = -1.14$, as shown in Fig. 5(f). The dotted bars at X^* and x^* indicate the superfluid transition points. Changes in f_P, f_n, $f_\mathcal{E}$, and f_μ and a cusp in $f_\mathcal{C}$ around the points can be seen. Such critical behavior can be seen at the normal to the superfluid transition point because of appearing the condensation energy [30]. [We have not identified the origin of the other cusps in $f_\mathcal{C}(x)$ around $x = -0.6$ and $x = -0.2$.]

While the Fermi system is nonzero temperature and the data show the phase transition, our experimental data can be well considered as the ground-state values. Deviations of the dimensionless thermodynamic quantities from the ground-state values due to finite-temperature effects such as the condensation energy and the thermal energy are estimated to be smaller than 1% at the unitarity limit and about 5% even for the BCS region in the normal state ($x < x^*$). The validity of the zero-temperature limit is discussed in Sec. IV C.

IV. DISCUSSIONS

A. Comparison with previous experiments and many-body theories

1. Isothermal compressibility: $f_\kappa(x)$

The obtained dimensionless compressibility is shown by the red circles in Fig. 6, along with previously obtained experimental data and a theoretical curve. The vertical axis follows a logarithmic scale.

At the unitarity limit, $f_\kappa(0) = 2.66(7)$ obtained in the preset study is consistent with a previously reported experimental value [2.66(3)], which was determined accurately by measuring the thermodynamics for homogeneous unitary Fermi gases [19]. The results for two different experiments are shown around the unitarity limit. One experiment measured density fluctuations [20]. The compressibility was determined based on density fluctuations according to the fluctuation-dissipation theorem. The other experiment measured the speed of sound propagating in the Fermi gas [21]. The speed of sound can be easily converted to isothermal compressibility, as shown in Eq. (21). While the results of these experiments are not the exact values for a homogeneous system because they were measured for a trapped system, the results of the present study show good qualitative agreement.

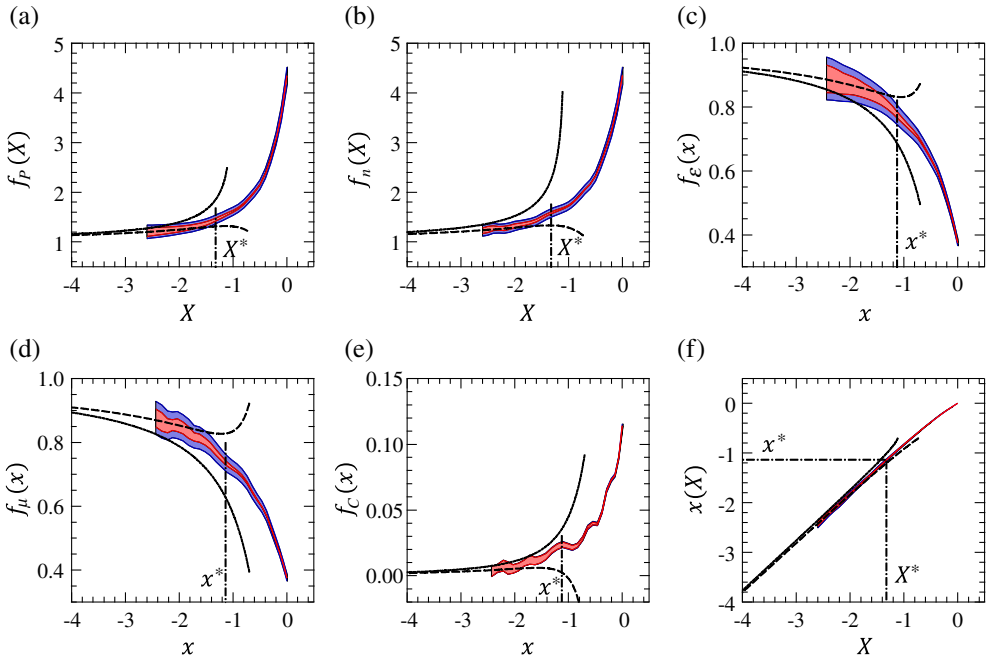

FIG. 5. Dimensionless thermodynamic functions derived from $\mathcal{G}(\chi)$. (a) Pressure. (b) Number density. (c) Internal energy density. (d) Chemical potential. (e) Contact density. (f) Canonical interaction parameter. The red colors indicate ranges of statistical errors caused by the uncertainty of the offset value of $\mathcal{G}(\chi)$. The blue colors indicate additional statistical errors resulting from the uncertainty of the absorption cross section. The dotted curves and the dashed curves show their asymptotic behavior at the BCS limit up to the first and second order of $1/x$, respectively. The vertical dash-dotted lines indicate interaction parameters X^* and x^* where superfluid transition occurs. The Fermi system is in the superfluid state in the region of $X > X^*$ or $x > x^*$.

The theoretical curve is calculated using an extended T-matrix approximation (ETMA) developed in a previous study [31,32] without using any fitting parameters. The theory excellently reproduces our experimental results in the superfluid region.

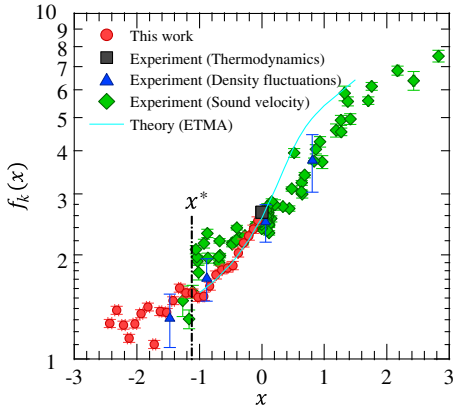

FIG. 6. Experimental and theoretical dimensionless isothermal compressibility. The vertical axis follows a logarithmic scale. The red circles indicate the experimental data of the present study. The green diamonds, blue triangles, and black square indicate experimental values obtained based on the speed of sound [21], density fluctuations [20], and thermodynamic measurements at the unitarity limit [19], respectively. The light blue curve indicates the theoretical calculation of ETMA [31,32]. The vertical dash-dotted line indicates the superfluid transition point x^* obtained in the present study.

2. *Pressure:* $f_P(X)$

The determined dimensionless pressure is shown by the red curve in Fig. 7, along with previous experimental data and a theoretical curve. The width of the red curve indicates the overall systematic error. The vertical axis follows a logarithmic scale.

Our value of $f_P(0) = 4.35(17)$ at the unitarity limit is consistent with the experimental value of 4.34(7), which is obtained by $f_P(0) = \xi^{-3/2}$, with $\xi = 0.376(4)$ determined using spin-balanced unitary Fermi gases in a previous study [19]. Our values from the BCS region to the unitarity limit agree qualitatively with the values determined using spin-imbalanced Fermi gases in a previous study [18], whereas our results are slightly larger. The ETMA [31,32] again reproduces our experimental results.

3. *Internal energy density:* $f_\mathcal{E}(x)$

The determined dimensionless internal energy density is shown by the red curve in Fig. 8, along with previous experimental data and various theoretical curves. The width of the red curve indicates the overall systematic errors.

At the unitarity limit, our value of $f_\mathcal{E}(0) = 0.375(10)$ agrees with the experimental value of 0.376(4) [19]. In a previous experiment [18], an approximated curve of $f_P^{\text{Padé}}(X)$ was prepared using the Padé approximation.

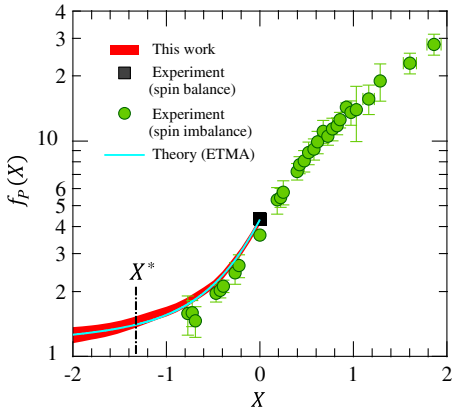

FIG. 7. Experimental and theoretical dimensionless pressure. The vertical axis follows a logarithmic scale. The red curve indicates the experimental data of the present study. The width indicates the total systematic error. The green circles and the black square indicate the experimental values obtained using spin imbalanced Fermi gases [18] and spin balanced unitary Fermi gas [19], respectively. The light blue curve indicates the theoretical calculation of the ETMA [31,32]. The vertical dash-dotted line indicates the superfluid transition point X^* of the present study.

An approximated curve $f_{\mathcal{E}}^{\text{Padé}}(x)$ was obtained from $f_P^{\text{Padé}}(X)$ using Eqs. (17) and (18), as shown by the dotted green curve. We find our data to be inconsistent with this approximated curve $f_{\mathcal{E}}^{\text{Padé}}(x)$.

The results of the ETMA [31,32] and the quantum Monte Carlo method [33] agree with our result within the error bars. A fixed-node diffusion Monte Carlo (FNDMC) method [34] and the Nozières and Schmitt-Rink (NSR) theory [35] provide larger values around the unitarity limit. A Luttinger-Ward (LW) approach [36] shows smaller values than our data around the unitarity limit.

4. Contact density: $f_{\mathcal{C}}(x)$

The obtained contact density is shown by the red curve in Fig. 9, along with previous experimental data and various theoretical curves. The width of the red curve indicates the overall systematic error. The vertical axis follows a logarithmic scale. The vertical dash-dotted line indicates the superfluid transition point at $x = x^*$.

In the previous experiment [17], contact density was measured using fermions in the normal state at $t = 0.18(2) \gtrsim t_c$ by radio frequency spectroscopy (rf line shape) and photon emission spectroscopy (PES). The temperature parameter is approximately 3 times higher than in our experimental condition. Nevertheless, the results of the present study agree quantitatively within the error bars, indicating that the short-range correlation is insensitive to both temperature and whether the many-body state is the normal state or the superfluid state.

We compare our results with the results of the FNDMC method [34], the NSR theory [37], the LW approach [38], the T-matrix approximation (TMA) [39], and ETMA [31,32]. All of these results agree quantitatively with our data in the BCS region.

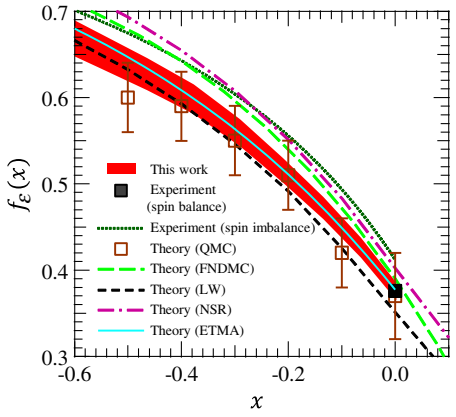

FIG. 8. Experimental and theoretical dimensionless internal energy density. The red curve indicates the experimental data of the present study in the superfluid state ($x > x^*$). The width indicates the total systematic error. The black square indicates the experimental data obtained using spin-balanced unitary Fermi gas [19], and the dotted green curve is an approximated curve based on pressure measurements of Ref. [18]. The light blue curve indicates the ETMA [31,32]. The open brown squares indicate data obtained by the QMC method [33]. The long dashed green curve was obtained by the FNDMC method [34]. The dash-dotted purple curve was obtained by the NSR theory [35]. The dashed black curve was obtained by the LW approach [36].

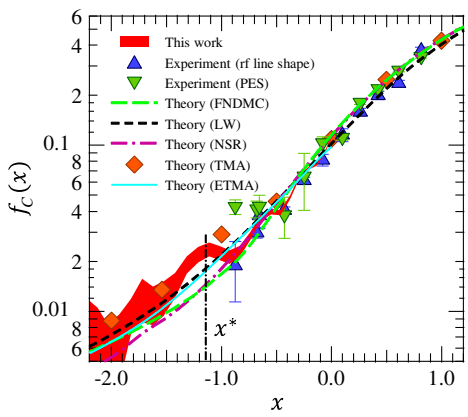

FIG. 9. Experimental and theoretical dimensionless contact density. The vertical axis follows a logarithmic scale. The red curve indicates the experimental data of the present study. The width indicates the total systematic errors. The blue triangles and the green inverse triangles indicate experimental values determined by radio frequency spectroscopy (rf line shape) and photon emission spectroscopy [17]. The light blue curve is the ETMA [31,32]. The long dashed green curve indicates the results obtained by the FNDMC method [34]. The dash-dotted purple curve indicates the results obtained by the NSR theory [37]. The short dashed black curve indicates the LW approach [38]. The brown diamonds indicate the results obtained by TMA [39].

B. Superfluid order parameter

In several strong-coupling theories, the order parameter Δ and chemical potential μ are calculated for given values of n and a by an equation obtained by combining a gap equation and a number equation. The gap equation is often approximated by the ordinary BCS gap equation [7,31,32,35,40,41], whereas the number equation is derived from the single-particle Green's function or the thermodynamic potential, which includes quantum fluctuations. In this case, Δ can be uniquely determined by the chemical potential of interacting fermions at $T = 0$. If this theoretical approach is adequate, we can calculate Δ by solving the gap equation with the chemical potential determined in the present study. Note that it is not obvious that the superfluid order parameter should satisfy the gap equation in the unitary regime. Nonetheless, it is interesting to evaluate Δ from thermodynamic quantities using the ordinary BCS gap equation and to compare it with values obtained by other methods.

The BCS gap equation at $T = 0$ is given by

$$-\frac{1}{a} = \frac{2}{\pi}\left(\frac{2m\Delta}{\hbar^2}\right)^{1/2} I_1\left(\frac{\mu}{\Delta}\right), \tag{29}$$

where the function $I_1(\mu/\Delta)$ is defined in a previous study [42]. When we define the dimensionless superfluid gap as

$$f_\Delta = \frac{\Delta}{\varepsilon_F(n)}, \tag{30}$$

the gap equation can be expressed in dimensionless form, relating x and f_Δ as

$$1 = -\frac{2}{\pi}\frac{\sqrt{f_\Delta}}{x} I_1\left(\frac{f_\mu(x)}{f_\Delta}\right). \tag{31}$$

Note that Δ and μ determined by the gap equation of Eq. (29) have the universal ratio of $\Delta/\mu = 1.16$ at the unitarity limit.

We substitute $f_\mu(x)$ determined in the superfluid range ($x > x^*$) into Eq. (31) and calculate f_Δ as a function of x. The result is shown by the red curve in Fig. 10. This curve essentially represents the relation among Δ, n, and a under the assumption that the gap equation holds true. The width of the red curve indicates the overall systematic error. The obtained values are close to the binding energy of the paired fermions directly observed by a spectroscopic experiment [14] as well as that obtained by the quantum Monte Carlo method [43,44]. Consequently, we find that the binding energy of the paired fermions can be simply estimated by substituting $f_\mu(x)$ into the gap equation. Note that the above observation does not indicate whether the magnitude of the order parameter obeys the gap equation, because the order parameter can deviate from the binding energy in the unitary regime. Direct measurement of the order parameter, such as the measurement of the Higgs mode, is desired in this regard [45].

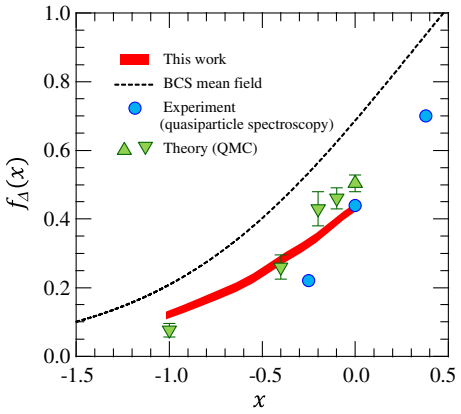

FIG. 10. Dimensionless superfluid gap. The red curve indicates the gap calculated by substituting our $f_\mu(x)$ into the gap equation in Eq. (31). The dashed black curve was obtained by BCS-MF calculation [42]. The green triangle and the green inverse triangles indicate the theoretical values obtained by the QMC method [43,44]. The blue circles are experimental values obtained by quasiparticle spectroscopy [14].

C. Validity of the experimental result

Here, we discuss the validity of the dilute condition, LDA, scale invariance, and zero-temperature limit for our experimental condition, and confirm that the determined dimensionless thermodynamic quantities show those for homogeneous fermions in the zero-temperature limit from the BCS region to the unitarity limit.

1. Dilute condition

The dilute condition is given by $r_0 \ll |a|, \lambda(T), k_F^{-1}, l_{\hat{\rho}}, l_{\hat{z}}$, where r_0 is the interaction potential size (van der Waals radius), $\lambda(T) = \sqrt{2\pi\hbar^2/mk_BT}$ is the thermal length, and $l_{\hat{\rho}} = \sqrt{\hbar/m\omega_{\hat{\rho}}}$ and $l_{\hat{z}} = \sqrt{\hbar/m\omega_{\hat{z}}}$ are the harmonic oscillation lengths in the radial and the axial directions, respectively. For our experimental conditions, $m = 1.0 \times 10^{-26}$ kg for ^{6}Li, $B = 832.18$–1050 G, $n \sim 1$ μm^{-3} (see Fig. 2), $T/T_F \sim 0.06$, $T \sim 24$ nK, $\omega_{\hat{\rho}}/2\pi \sim 250$ Hz, and $\omega_{\hat{z}}/2\pi \sim 7$ Hz, where $\omega_{\hat{\rho}}$ is the approximate trapping frequency along the radial direction, each length in the system is $r_0 = 1.6$ nm for ^{6}Li [25], $|a| = 185\,\text{nm} \sim \infty$, $\lambda = 730$ nm, $k_F^{-1} = 320$ nm, $l_{\hat{\rho}} = 16$ μm, and $l_{\hat{z}} = 100$ μm. Therefore, the dilute condition is satisfied.

2. Local density approximation

The LDA is valid under the condition of $k_F^{-1}, \lambda(T), \xi_{\text{pair}} \ll l_{\hat{\rho}}, l_{\hat{z}}$ for the superfluid fermions and $k_F^{-1}, \lambda(T) \ll l_{\hat{\rho}}, l_{\hat{z}}$ for the normal fermions [46], where ξ_{pair} is the fermion pair size. In this experiment, the superfluid transition point occurs at $x^* \sim -1$ due to the nonzero

temperature of the fermions. For this interaction parameter, the superfluid gap is estimated to be $\Delta \sim 0.1\varepsilon_F$ from Fig. 10. We estimate the fermion pair size by the Pippard coherence length by $\xi_{\rm pair} = [\hbar v_F(n)]/(\pi\Delta)$ [47], where $v_F(n) = \hbar k_F(n)/m$ is the Fermi velocity. At the critical point, the value is $\xi_{\rm pair} = 2\ \mu$m. This value gives the upper limit of the fermion pair size for superfluid fermions realized in this experiment because the gap has smaller values at smaller interaction parameter values. As a result, all the conditions for the LDA are satisfied in the superfluid region and the normal region.

We also note that the trapping energy does not prevent pairing near $x = x^*$ in this experiment because the inequality $\Delta > \hbar\omega_{\hat{\rho}}, \hbar\omega_{\hat{z}}$ is satisfied at the critical point. The superfluid-normal transition we observe in this experiment results from the nonzero temperature of the fermions.

3. Scale invariance

Scale invariance can be satisfied at the local position of the trapping system, if both the dilute condition and the LDA are satisfied. As discussed above, both conditions are satisfied. Therefore, scale invariance is a valid assumption at the local position of the three-dimensional trapping system in our experimental condition.

4. Zero-temperature limit

The estimated temperature parameter of the experimental data used in data analysis is a small value of $0.06 \lesssim t_{\rm expt} \lesssim 0.1$. At the unitarity limit, it is valid to consider that the fermions are in the ground state because the superfluid fraction is expected to be unity at this temperature parameter [19,48]. Therefore, the systematic errors in the unitary regime are determined only by the uncertainty of the absorption cross section $\sigma_{\rm abs}$.

Outside of the unitarity limit, however, there are systematic errors caused by finite-temperature effects in $f_P(X)$ because the superfluid density becomes smaller at smaller X. When there are normal components, it works to increase the pressure due to the thermal energy by $\delta f_P^T > 0$, and also it works to decrease the pressure due to loss of the condensation energy by $\delta f_P^\Delta(X) > 0$. Therefore, the exact value in the ground state $f_P^g(X)$ is given by $f_P^g(X) = f_P(X) - \delta f_P^T + \delta f_P^\Delta(X)$, and the upper and the lower limit of the relative error is given by $-[\delta f_P^\Delta(X)/f_P^g(X)] < \delta_P(X) < [\delta f_P^T(X)/f_P^g(X)]$, where $\delta_P(X) \equiv [f_P(X) - f_P^g(X)/f_P^g(X)]$.

While we need to evaluate the systematic errors experimentally, it is beyond the scope of this work. Here, we estimate the possible errors at the level of the BCS mean-field approximation. Under the approximation, they are estimated by $\delta f_P^T = (5\pi^2/12)t^2$ and $\delta f_P^\Delta(X) = (15/16)f_\Delta^2(X)$ [22]. We also assume $f_P^g(X) \approx f_P(X) \gg \delta f_P^T(X), \delta f_P^\Delta(X)$. Then we find that $[\delta f_P^T(X)/f_P^g(X)]$ has the maximum value of 0.02 at $X = -\infty$, and $[\delta f_P^\Delta(X)/f_P^g(X)]$ has the maximum value of 0.04 at $X = 0$ from the BCS limit to the unitarity limit. Hence, the range of the systematic error in the measured $f_P(X)$ is estimated to be $-4\% < \delta_P(X) < 2\%$ from the BCS region to the unitarity limit. It gives the range of the systematic error in $f_\mathcal{E}(x)$ from the exact value in the ground state $f_\mathcal{E}^g(x)$ as $-1\% < \delta_\mathcal{E}(x) < 3\%$ by using general thermodynamic properties, where $\delta_\mathcal{E}(x) \equiv [f_\mathcal{E}(x) - f_\mathcal{E}^g(x)/f_\mathcal{E}^g(x)]$. Details are described in Appendix B.

Consequently, these small relative errors mean that the experimentally determined dimensionless thermodynamic values can be considered as the values at the zero-temperature limit from the BCS region to the unitarity limit.

V. CONCLUSION

This paper reports experimental determination of thermodynamic quantities for homogeneous fermions interacting with an s-wave scattering length in the zero-temperature limit from the BCS region to the unitarity limit. They are determined by using standard thermodynamic relations, the scale-invariant property, and the local density approximation. In previous works, the number of data points in the BCS region was not adequate to understand many-body physics [18]. The BCS region is of interest in electron systems, nuclear physics, etc. In order to increase the number of high-accuracy data points in the BCS region, we develop a new method to determine the chemical potential of spin-balanced Fermi gases. As a result, the data density in the BCS region has been significantly improved, and various thermodynamic quantities are directly derived without using model functions such as the Padé approximation. In particular, we determine $f_\mathcal{E}(x)$ for internal energy density directly from experimental data.

All of the quantities are determined within systematic errors of 4% around the unitarity limit. Consequently, we are able to evaluate the many-body theory and find the extended T-matrix approximation as a valid theory. The ETMA, which is a strong-coupling theory involving fluctuations in the Cooper channel, provides the closest results to those of the present study. Our results will promote the understanding of superfluid fluctuations on the thermodynamic quantities of the superfluid Fermi gas. The details of the ETMA can be found in previous studies [31,32,41].

In addition, our paper includes new findings about the relationship between the thermodynamic quantities and the superfluid gap. Future experiments, such as experiments involving the measurement of the Higgs mode of the order parameter, will reveal the magnitude of the order parameter as well as the relation between the order parameter and the binding energy.

The s-wave interacting Fermi gas is an effective model, beyond the free-Fermi gas model, which describes interacting Fermi systems qualitatively. This study certainly

advances the quantum many-body physics beyond atomic, molecular, and optical physics. We introduce two specific examples of application of this experimental result in condensed-matter physics and nuclear physics.

(i) The mechanism of the high-temperature (high-T_c) superconductivity by using the BCS-BEC crossover conjecture has been discussed since Eagles's theoretical work in 1969 [49]. The BCS-BEC crossover physics is still considered as a valid theoretical framework for high-T_c superconductivity qualitatively, whereas there are lattice and Coulomb interactions in electron systems [50,51]. Recently, it has been found that the electron system of FeSe has a surprisingly large superconducting gap of $\Delta/\varepsilon_F \sim 1$ in the superconducting state [52]. In addition, it has been confirmed that superconducting fluctuations significantly affect the physical properties of the superconducting state [53]. It is expected that the FeSe system can be near the unitary regime because of such large pairing gap and large fluctuations. By comparing such electron systems with cold Fermi gases, for example, the relation between the chemical potential and the gap energy, we can distinguish universal physics and specific physics in the FeSe system. It may lead to elucidation of the mechanism of high-temperature superconductivity in FeSe and other high-T_c materials.

(ii) The dilute nucleon system is a nonrelativistic four-component (spin-1/2 and isospin-1/2) Fermi gas of neutrons and protons at zero temperature. Their interaction can be considered as s-wave scattering in the dilute system. The s-wave scattering lengths between a proton and a neutron are determined to be $a_t \simeq 5.4$ fm in the $^3S_1$ channel with a shallow bound state of the deuteron, and $a_s \simeq -23.7$ fm in the $^3S_1$ channel [54]. The neutron-neutron scattering length is also determined to be $a_{NN} = -18.63$ fm [55]. While these scattering lengths are constant values, the interaction parameters $x = 1/k_F(n)a$ depend on the particle density, and they reach the unitary regime at densities around $n_0/10$, where $n_0 = 0.16$ fm^{-3} is the nuclear saturation densities. In particular, the equation of state of neutron matter, which is a relation between the neutron density and the internal energy, is important in nuclear physics in terms of the symmetry energy of nuclei, neutron skin thickness of neutron-rich nuclei, and physical properties of neutron stars [56–58]. While there are dilute neutron systems in the neutron skin or neutron halo of neutron-rich nuclei [59,60] and the tetra-neutron state [61], it is generally difficult to prepare dilute nucleon matter on Earth directly. Therefore, experimental simulation of such a dilute nucleon system using cold Fermi atomic gases is essential to understand the elemental physics such as thermodynamics, the equation of state, and the pairing gap. Thus far, there have been no experimental studies to test nuclear theories at low densities. This study enables us to confirm the validity of nuclear theories at low densities.

ACKNOWLEDGMENTS

We would like to thank N. Navon, C. Salomon, C. Sanner, W. Ketterle, J. Thomas, T. E. Drake, and D. Jin for providing their experimental data, R. Haussmann, W. Zwerger, H. Hu, G. C. Strinati, A. Gezerlis, S. Gandolfi, and J. Carlson for providing their theoretical calculations, and W. Zwerger for valuable discussions about the critical behavior of contact density around the superfluid transition point. M. H. would like to thank Y. Aratake for assistance in conducting the experiments. H. T. and Y. O. would like to thank P. van Wyk, R. Hanai, D. Kagamihara, and D. Inotani for their useful discussions. The present study was supported by a Grant-in-Aid for Scientific Research on Innovative Areas (No. 24105006) and by a Grant-in-Aid for Young Scientists (A) (No. 23684033). H. T. was supported by a Grant-in-Aid for JSPS Fellows. Y. O. was supported by the KiPAS project of Keio University as well as by Grants-in-Aid for Scientific Research from MEXT and JSPS (No. 15H00840, No. 15K00178, and No. 16K05503).

APPENDIX A: SUPERFLUID TRANSITION POINT AND EXPERIMENTAL TEMPERATURE

Experimentally, it is impossible to prepare fermions at zero temperature, even if we start from a molecular BEC, and so fermions are always prepared at finite temperature. In the case of Fermi systems, it is proper to discuss temperature in terms of a temperature parameter defined as $t = k_B T/\varepsilon_F$. When investigating the properties of interacting fermions in the ground state, the experimental temperature t_{expt} should not only be sufficiently lower than 1 in order to exclude temperature and entropy from the thermodynamics, but should also be lower than the superfluid critical temperature t_c to take into account the condensation energy [30]. Therefore, $t_{\mathrm{expt}} < t_c < 1$ should be satisfied in order to investigate the ground state. Since t_c decreases monotonically to zero from the unitarity limit to the BCS limit as a function of the interaction parameter x, it is inevitable that $t_c(x)$ intersects t_{expt} somewhere between the two interaction limits. Here, we define the intersection as $t_{\mathrm{expt}} = t_c(x^*)$.

We determine the superfluid transition point x^* by measuring the condensate fraction (CF) of paired fermions. The value of x^* can be determined even if we know neither the experimental temperature t_{expt} nor the function for the critical temperature $t_c(x)$. Since the local density has a peak value at the bottom of the trap, the ratio t_{expt}/t_c takes the minimum value there. Therefore, CF takes finite values when fermions satisfy $t_{\mathrm{expt}}/t_c < 1$ at the bottom, and CF becomes zero at $t_{\mathrm{expt}} = t_c(x^*)$.

We carry out the measurement of CF as follows. We prepare ultracold fermions at various magnetic fields for the Feshbach resonance using the same experimental procedure as in the present study. Instead of measuring the

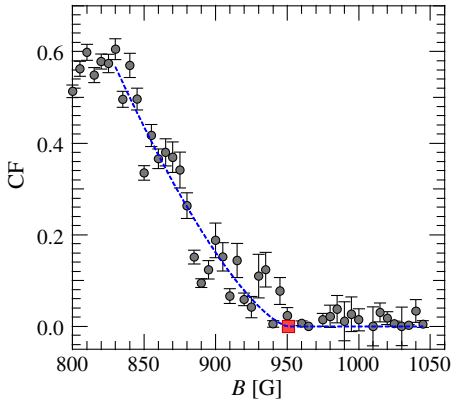

FIG. 11. Condensate fraction of paired fermions evaluated at various magnetic fields for the Feshbach resonance. The circles with error bars indicate experimental data. The dashed curve shows the fitting result. The red square corresponds to the point at which the condensate fraction disappears.

in situ column density of the fermions, we measure the center-of-mass (c.m.) momentum distribution of the paired fermions [23]. We turn off the ODT and the magnetic field simultaneously within 10 μs. At that time, the paired fermions are converted to molecules because the Fermi system is changed to the BEC regime. These molecules expand with the original c.m. momentum distribution of the paired fermions during time of flight. We measure the momentum distribution after a time of flight of 11 ms by absorption imaging.

Figure 11 shows the CF evaluated by fitting a bimodal function to the measured momentum distribution. In order to estimate the magnetic field B^*, at which CF becomes zero, we fit an empirical function of $\mathrm{CF} = a(B^* - B)^b\Theta(B^* - B)$ to the data with fitting parameters B^*, a, and b. The fitting result yields $B^* = 951$ G. We then evaluate the value of x^* by $x^* = [1/k_F(n)a(B^*)]$ with the peak density and the scattering length at the magnetic field. In this way, the superfluid transition point is determined to be $x^* = -1.14$. In the region of $x > x^*$, fermions are in the superfluid state.

Next, we estimate the experimental temperature t_{expt}. At the unitarity limit (832.18 G), we observe a condensate fraction of 0.6, as shown in Fig. 11. This suggests that $t_{\mathrm{expt}} < 0.1$ at $x = 0$, according to a previous experimental result [19]. At $x^* = -1.14$, the critical temperature is calculated to be $t_c(x^*) = 0.06$ [36]. Since $t_{\mathrm{expt}} = t_c(x^*)$, we estimate $t_{\mathrm{expt}} \sim 0.06$ at $x = -1.14$. At $x < -1.14$, it is difficult to estimate the temperature parameter from our experimental data. According to a theoretical work of Ref. [62], the temperature parameter at the trap center decreases during an adiabatic change from the BEC region to the BCS region along the isentropic curve. Consequently, we estimate the temperature parameter to be $0.06 \lesssim t_{\mathrm{expt}} \lesssim 0.1$ from around the BCS region to the unitarity limit.

APPENDIX B: ESTIMATION OF THE RELATIVE ERROR OF $f_{\mathcal{E}}(x)$

We can estimate the range of the relative error of $f_{\mathcal{E}}(x)$ from upper and lower bounds $-\delta_P^- \le \delta_P(X) \le \delta_P^+$ of the relative error of $f_P(X)$ by using general thermodynamic properties.

There is an exact thermodynamic relation given by $P^g(\mu^g(n)) = n\mu^g(n) - \mathcal{E}^g(n)$ at a given density n at the ground state, where "g" in the superscript means thermodynamic values at the ground state. Since $P^g(\mu)$ is a downward-convex function due to mechanical stability ($\kappa^g > 0$), an inequality of $P^g(\mu) \ge n\mu - \mathcal{E}^g(n)\ \forall\ \mu$ is satisfied. When a lower bound on the measured pressure is given by $P(\mu) \ge (1-\delta_P^-)P^g(\mu)\ \forall\ \mu$, it leads to $P(\mu) \ge (1-\delta_P^-)[(n/1-\delta_P^-)\mu - \mathcal{E}^g(n/1-\delta_P^-)]\ \forall\ \mu$ by using the inequality of $P^g(\mu)$ with density $(n/1-\delta_P^-)$. It reduces to $P(\mu) \ge n\mu - (1-\delta_P^-)\mathcal{E}^g(n/1-\delta_P^-)\ \forall\ \mu$. Since the functions $\mathcal{E}(n)$ and $\mu(n)$ derived from $P(\mu)$ should satisfy $P(\mu) = n\mu(n) - \mathcal{E}(n)$, we have $\mathcal{E}(n) \le (1-\delta_P^-)\mathcal{E}^g(n/1-\delta_P^-)\ \forall\ n$. Then we obtain $\mathcal{E}(n) - \mathcal{E}^g(n) \lesssim \delta_P^- P^g(\mu^g(n)) \le \frac{2}{3}\delta_P^-\mathcal{E}^g(n)$, where we use an inequality of $P^g(\mu^g(n)) \le \frac{2}{3}\mathcal{E}^g(n)$ for $a \le 0$ due to the universal pressure-energy relation [8–13]. We thus arrive at $\delta_{\mathcal{E}}(x) \le \frac{2}{3}\delta_P^-$. Since the lower bound on the measured pressure is given by $\delta_P^- = (\delta f_P^{\Delta}/f_P^g) = 4\%$, we have an upper bound on the internal energy density as $\delta_{\mathcal{E}} \le 3\%$.

Next, suppose that an upper bound on the measured pressure is given by $P(\mu) \le (1+\delta_P^+)P^g(\mu)\ \forall\ \mu$. Since the measured pressure $P(\mu)$ is also a downward-convex function, we have $P(\mu) \ge n\mu - \mathcal{E}(n)\ \forall\ \mu$. Considering a specific case of $\mu = \mu^g(n)$, we have $n\mu^g(n) - \mathcal{E}(n) \le (1+\delta_P^+)P^g(\mu^g(n))\ \forall\ n$. As a result, we get $\delta_{\mathcal{E}}(x) \ge -\frac{2}{3}\delta_P^+$. Since the upper bound of the measured pressure is given by $\delta_P^+ = (\delta f_P^T/f_P^g) = 2\%$, we have a lower bound on the internal energy density as $\delta_{\mathcal{E}} \ge -1\%$.

As a result, the boundary of the relative error of $f_{\mathcal{E}}(x)$ can be estimated to be $-1\% \le \delta_{\mathcal{E}}(x) \le 3\%$ from the BCS region to the unitarity limit.

[1] W. Zwerger, *The BCS-BEC Crossover and the Unitary Fermi Gas* (Springer Science & Business Media, Berlin, Heidelberg, 2011), Vol. 836.
[2] S. Giorgini, L. P. Pitaevskii, and S. Stringari, *Theory of Ultracold Atomic Fermi Gases*, Rev. Mod. Phys. **80**, 1215 (2008).
[3] I. Bloch, J. Dalibard, and W. Zwerger, *Many-Body Physics with Ultracold Gases*, Rev. Mod. Phys. **80**, 885 (2008).
[4] C. Chin, R. Grimm, P. Julienne, and E. Tiesinga, *Feshbach Resonances in Ultracold Gases*, Rev. Mod. Phys. **82**, 1225 (2010).
[5] T.-L. Ho, *Universal Thermodynamics of Degenerate Quantum Gases in the Unitarity Limit*, Phys. Rev. Lett. **92**, 090402 (2004).

[6] A. J. Leggett, *Quantum Liquids: Bose Condensation and Cooper Pairing in Condensed-Matter Systems* (Oxford University Press, New York, 2006).

[7] R. B. Diener, R. Sensarma, and M. Randeria, *Quantum Fluctuations in the Superfluid State of the BCS-BEC Crossover*, Phys. Rev. A **77**, 023626 (2008).

[8] S. Tan, *Energetics of a Strongly Correlated Fermi Gas*, Ann. Phys. (Amsterdam) **323**, 2952 (2008).

[9] S. Tan, *Large Momentum Part of a Strongly Correlated Fermi Gas*, Ann. Phys. (Amsterdam) **323**, 2971 (2008).

[10] S. Tan, *Generalized Virial Theorem, and Pressure Relation for a Strongly Correlated Fermi Gas*, Ann. Phys. (Amsterdam) **323**, 2987 (2008).

[11] E. Braaten, D. Kang, and L. Platter, *Universal Relations for a Strongly Interacting Fermi Gas Near a Feshbach Resonance*, Phys. Rev. A **78**, 053606 (2008).

[12] S. Zhang and A. J. Leggett, *Universal Properties of the Ultracold Fermi Gas*, Phys. Rev. A **79**, 023601 (2009).

[13] F. Werner and Y. Castin, *General Relations for Quantum Gases in Two and Three Dimensions: Two-Component Fermions*, Phys. Rev. A **86**, 013626 (2012).

[14] A. Schirotzek, Y.-i. Shin, C. H. Schunck, and W. Ketterle, *Determination of the Superfluid Gap in Atomic Fermi Gases by Quasiparticle Spectroscopy*, Phys. Rev. Lett. **101**, 140403 (2008).

[15] Y. Sagi, T. E. Drake, R. Paudel, and D. S. Jin, *Measurement of the Homogeneous Contact of a Unitary Fermi Gas*, Phys. Rev. Lett. **109**, 220402 (2012).

[16] Y. Sagi, T. E. Drake, R. Paudel, R. Chapurin, and D. S. Jin, *Probing Local Quantities in a Strongly Interacting Fermi Gas*, J. Phys. Conf. Ser. **467**, 012010 (2013).

[17] Y. Sagi, T. E. Drake, R. Paudel, R. Chapurin, and D. S. Jin, *Breakdown of the Fermi Liquid Description for Strongly Interacting Fermions*, Phys. Rev. Lett. **114**, 075301 (2015).

[18] N. Navon, S. Nascimbène, F. Chevy, and C. Salomon, *The Equation of State of a Low-Temperature Fermi Gas with Tunable Interactions*, Science **328**, 729 (2010).

[19] M. J. H. Ku, A. T. Sommer, L. W. Cheuk, and M. W. Zwierlein, *Revealing the Superfluid Lambda Transition in the Universal Thermodynamics of a Unitary Fermi Gas*, Science **335**, 563 (2012).

[20] C. Sanner, E. J. Su, A. Keshet, W. Huang, J. Gillen, R. Gommers, and W. Ketterle, *Speckle Imaging of Spin Fluctuations in a Strongly Interacting Fermi Gas*, Phys. Rev. Lett. **106**, 010402 (2011).

[21] J. Joseph, B. Clancy, L. Luo, J. Kinast, A. Turlapov, and J. E. Thomas, *Measurement of Sound Velocity in a Fermi Gas Near a Feshbach Resonance*, Phys. Rev. Lett. **98**, 170401 (2007).

[22] A. L. Fetter and J. D. Walecka, *Quantum Theory of Many-Particle Systems* (Dover Publications, Inc., Mineola, New York, 2003).

[23] T. Ikemachi, A. Ito, Y. Aratake, Y. Chen, M. Koashi, M. Kuwata-Gonokami, and M. Horikoshi, *All-Optical Production of Dual Bose-Einstein Condensates of Paired Fermions and Bosons with* ^{6}Li *and* ^{7}Li, J. Phys. B **50**, 01LT01 (2017).

[24] G. Zürn, T. Lompe, A. N. Wenz, S. Jochim, P. S. Julienne, and J. M. Hutson, *Precise Characterization of* ^{6}Li *Feshbach Resonances Using Trap-Sideband-Resolved rf Spectroscopy of Weakly Bound Molecules*, Phys. Rev. Lett. **110**, 135301 (2013).

[25] P. S. Julienne and J. M. Hutson, *Contrasting the Wide Feshbach Resonances in* ^{6}Li *and* ^{7}Li, Phys. Rev. A **89**, 052715 (2014).

[26] M. Horikoshi, A. Ito, T. Ikemachi, Y. Aratake, M. Kuwata-Gonokami, and M. Koashi, *Appropriate Probe Condition for Absorption Imaging of Ultracold* ^{6}Li *Atoms*, J. Phys. Soc. Jpn. **86**, 104301 (2017).

[27] T.-L. Ho and Q. Zhou, *Obtaining the Phase Diagram and Thermodynamic Quantities of Bulk Systems from the Densities of Trapped Gases*, Nat. Phys. **6**, 131 (2010).

[28] F. Werner and M. Zwierlein (unpublished).

[29] S. Nascimbène, N. Navon, F. Chevy, and C. Salomon, *The Equation of State of Ultracold Bose and Fermi Gases: A Few Examples*, New J. Phys. **12**, 103026 (2010).

[30] N. Navon, S. Nascimbène, X. Leyronas, F. Chevy, and C. Salomon, *Condensation Energy of a Spin-*$1/2$ *Strongly Interacting Fermi Gas*, Phys. Rev. A **88**, 063614 (2013).

[31] H. Tajima, R. Hanai, and Y. Ohashi, *Strong-Coupling Corrections to Spin Susceptibility in the BCS-BEC-Crossover Regime of a Superfluid Fermi Gas*, Phys. Rev. A **93**, 013610 (2016).

[32] H. Tajima, P. van Wyk, R. Hanai, D. Kagamihara, D. Inotani, M. Horikoshi, and Y. Ohashi, *Strong-Coupling Corrections to Ground-State Properties of a Superfluid Fermi Gas*, Phys. Rev. A **95**, 043625 (2017).

[33] A. Bulgac, J. E. Drut, and P. Magierski, *Quantum Monte Carlo Simulations of the BCS-BEC Crossover at Finite Temperature*, Phys. Rev. A **78**, 023625 (2008).

[34] S. Gandolfi, K. E. Schmidt, and J. Carlson, *BEC-BCS Crossover and Universal Relations in Unitary Fermi Gases*, Phys. Rev. A **83**, 041601 (2011).

[35] H. Hu, X.-J. Liu, and P. D. Drummond, *Equation of State of a Superfluid Fermi Gas in the BCS-BEC Crossover*, Europhys. Lett. **74**, 574 (2006).

[36] R. Haussmann, W. Rantner, S. Cerrito, and W. Zwerger, *Thermodynamics of the BCS-BEC Crossover*, Phys. Rev. A **75**, 023610 (2007).

[37] E. D. Kuhnle, H. Hu, X.-J. Liu, P. Dyke, M. Mark, P. D. Drummond, P. Hannaford, and C. J. Vale, *Universal Behavior of Pair Correlations in a Strongly Interacting Fermi Gas*, Phys. Rev. Lett. **105**, 070402 (2010).

[38] R. Haussmann, M. Punk, and W. Zwerger, *Spectral Functions and rf Response of Ultracold Fermionic Atoms*, Phys. Rev. A **80**, 063612 (2009).

[39] F. Palestini, A. Perali, P. Pieri, and G. C. Strinati, *Temperature and Coupling Dependence of the Universal Contact Intensity for an Ultracold Fermi Gas*, Phys. Rev. A **82**, 021605 (2010).

[40] K. Levin, Q. Chen, C.-. Chien, and Y. He, *Comparison of Different Pairing Fluctuation Approaches to BCS-BEC Crossover*, Ann. Phys. (Amsterdam) **325**, 233 (2010).

[41] H Tajima, P van Wyk, R Hanai, D Kagamihara, D Inotani, M Horikoshi, and Y Ohashi, *Zero-Temperature Properties of a Strongly Interacting Superfluid Fermi Gas in the BCS-BEC Crossover Region*, J. Low Temp. Phys. **187**, 677 (2017).

[42] M. Marini, F. Pistolesi, and G. C. Strinati, *Evolution from BCS Superconductivity to Bose Condensation: Analytic*

Results for the Crossover in Three Dimensions, Eur. Phys. J. B **1**, 151 (1998).

[43] J. Carlson and S. Reddy, *Asymmetric Two-Component Fermion Systems in Strong Coupling*, Phys. Rev. Lett. **95**, 060401 (2005).

[44] A. Gezerlis and J. Carlson, *Strongly Paired Fermions: Cold Atoms and Neutron Matter*, Phys. Rev. C **77**, 032801 (2008).

[45] R. G. Scott, F. Dalfovo, L. P. Pitaevskii, and S. Stringari, *Rapid Ramps across the BEC-BCS Crossover: A Route to Measuring the Superfluid Gap*, Phys. Rev. A **86**, 053604 (2012).

[46] M. Houbiers, R. Ferwerda, H. T. C. Stoof, W. I. McAlexander, C. A. Sackett, and R. G. Hulet, *Superfluid State of Atomic* ^{6}Li *in a Magnetic Trap*, Phys. Rev. A **56**, 4864 (1997).

[47] C. H. Schunck, Y.-i. Shin, A. Schirotzek, and W. Ketterle, *Determination of the Fermion Pair Size in a Resonantly Interacting Superfluid*, Nature (London) **454**, 739 (2008).

[48] L. A. Sidorenkov, M. K. Tey, R. Grimm, Y.-H. Hou, L. Pitaevskii, and S. Stringari, *Second Sound and the Superfluid Fraction in a Fermi Gas with Resonant Interactions*, Nature (London) **498**, 78 (2013).

[49] D. M. Eagles, *Possible Pairing without Superconductivity at Low Carrier Concentrations in Bulk, and Thin-Film Superconducting Semiconductors*, Phys. Rev. **186**, 456 (1969).

[50] A. J. Leggett, *What Do We Know about High* T_c*?*, Nat. Phys. **2**, 134 (2006).

[51] P. Magierski, G. Wlazłowski, and A. Bulgac, *Onset of a Pseudogap Regime in Ultracold Fermi Gases*, Phys. Rev. Lett. **107**, 145304 (2011).

[52] S. Kasahara, T. Watashige, T. Hanaguri, Y. Kohsaka, T. Yamashita, Y. Shimoyama, Y. Mizukami, R. Endo, H. Ikeda, K. Aoyama *et al.*, *Field-Induced Superconducting Phase of FeSe in the BCS-BEC Cross-Over*, Proc. Natl. Acad. Sci. U.S.A. **111**, 16309 (2014).

[53] S. Kasahara, T. Yamashita, A. Shi, R. Kobayashi, Y. Shimoyama, T. Watashige, K. Ishida, T. Terashima, T. Wolf, F. Hardy *et al.*, *Giant Superconducting Fluctuations in the Compensated Semimetal FeSe at the BCS-BEC Crossover*, Nat. Commun. **7**, 12843 (2016).

[54] S. König, H. W. Grießhammer, H.-W. Hammer, and U. van Kolck, *Nuclear Physics around the Unitarity Limit*, Phys. Rev. Lett. **118**, 202501 (2017).

[55] Q. Chen *et al.*, *Measurement of the Neutron-Neutron Scattering Length Using the* $\pi^- d$ *Capture Reaction*, Phys. Rev. C **77**, 054002 (2008).

[56] J. Carlson, A. Gezerlis, and S. Reddy, *Equation of State and Pairing Gaps in Cold Atoms and Low-Density Neutron Matter*, AIP Conf. Proc. **995**, 17 (2008).

[57] S. Gandolfi, J. Carlson, S. Reddy, A. W. Steiner, and R. B. Wiringa, *The Equation of State of Neutron Matter, Symmetry Energy and Neutron Star Structure*, Eur. Phys. J. A **50**, 10 (2014).

[58] J. M. Lattimer, *The Nuclear Equation of State, and Neutron Star Masses*, Annu. Rev. Nucl. Part. Sci. **62**, 485 (2012).

[59] K. Hebeler, J. D. Holt, J. Menndez, and A. Schwenk, *Nuclear Forces and Their Impact on Neutron-Rich Nuclei and Neutron-Rich Matter*, Annu. Rev. Nucl. Part. Sci. **65**, 457 (2015).

[60] J. Margueron, H. Sagawa, and K. Hagino, *BCS-BEC Crossover of Neutron Pairs in Symmetric and Asymmetric Nuclear Matter*, Phys. Rev. C **76**, 064316 (2007).

[61] K. Kisamori *et al.*, *Candidate Resonant Tetraneutron State Populated by the* ^{4}He(^{8}He,^{8}Be) *Reaction*, Phys. Rev. Lett. **116**, 052501 (2016).

[62] Q. Chen, J. Stajic, and K. Levin, *Thermodynamics of Interacting Fermions in Atomic Traps*, Phys. Rev. Lett. **95**, 260405 (2005).